Constraints on the Formation of the Planet In HD 188753

Hannah Jang-Condell

Carnegie Institution of Washington, Department of Terrestrial Magnetism

5241 Broad Branch Road NW, Washington, D.C. 20015

hannah@dtm.ciw.edu

ABSTRACT

The claimed discovery of a Jupiter-mass planet in the close triple star system HD 188753 poses a problem for planet formation theory. A circumstellar disk around the planet's parent star would be truncated close to the star, leaving little material available for planet formation. In this paper, we attempt to model a protoplanetary disk around HD 188753A using a fairly simple α-disk model, exploring a range of parameters constrained by observations of T Tauri-type stars. The disk is truncated to within 1.5 to 2.7 AU, depending on model parameters. We find that the in situ formation of the planet around HD 188753A is implausible.

Subject headings: stars: individual (HD 188753) — planetary systems: protoplanetary disks — planetary systems: formation

1. Introduction

Recently, Konacki (2005) has claimed the detection of a short-period Jupiter-mass planet in the close triple system HD 188753. The most luminious member, HD 188753A (1.06 $M_\odot$), hosts the planet, and its companion, HD 188753B, orbiting at a semi-major axis of 12.3 AU, is actually a spectroscopic binary itself, with total mass 1.63 $M_\odot$. While the planet is a typical "hot Jupiter," with a minimum mass of 1.14 M_J and orbital period of 3.35 days, its existence in such a close binary system is exceptional. With an eccentricity of 0.5, the B component is 6 AU from the A component at closest approach, which would severely truncate a protoplanetary disk around A. A study of test particle orbits indicates that the disk should be truncated at 1.3 AU (Pichardo et al. 2005; Konacki 2005). However, analysis of Lindblad resonances in gaseous disks in eccentric binary systems suggest that the disk might extend somewhat further out, depending on the disk's Reynolds number (Artymowicz

& Lubow 1994, henceforth AL). In any case, the circumstellar disk will be truncated well within 6 AU. Given such a small disk, could the 1.14 M_J planet around HD 188753 have formed in situ?

For the purposes of this paper, we adopt an α-disk model that includes heating both from viscous accretion and stellar irradiation from the central star. The advantage of using such a model is that the properties of the disk are controlled by a handful of parameters, even though the microphysics of the processes are not fully modelled. In the case of a circumstellar disk around an isolated star, these models provide good fits to observed SEDs (D'Alessio et al. 2001). In a binary system, the companion object can substantially distort the disk, creating non-axisymmetries and spiral structures. Adequately modelling these phenomena requires high resolution hydrodynamic simulations, which are time-consuming and computationally intensive. The objective of this paper is to establish limits on the feasibility of in situ planet formation in HD 188753 without resorting to such simulations, hence we adopt a simple α-disk model, exploring a range of disk parameters to put limits on the possibility of planet formation. Shock heating from the generation of spiral structure in the disk is likely to inhibit rather than encourage planet formation (Nelson 2000; Mayer et al. 2005), so showing that planet formation cannot occur in the more quiescent α-disk model puts a strong constraint on planet formation in HD 188753.

Other workers have studied the possibility that HD 188753 formed in a crowded stellar environment and that the planet's presence around the A component is a result of dynamical interactions. Pfahl (2005) and Portegies Zwart & McMillan (2005) agree that the most likely scenario is that the planet formed around A, which then swapped into a pre-existing hierarchical triple system. In this paper, we support this scenario by ruling out in situ formation of the planet.

Although there is some debate about exactly how planets form, whether by core accretion (e.g. Pollack et al. 1996; Chambers 2004) or disk instability (e.g. Boss 1997, 2000, 2001), it is generally accepted that planets form out of disks of circumstellar material accreting onto the star. A truncated disk around HD 188753A puts severe limits on the amount of material that could be available for planet formation. In this paper, we explore the possibilities of planet formation in such a disk. The disk models used in this paper are based on established α-disk models for T Tauri stars, which are the prototypes for protoplanetary disks (Calvet et al. 1991; D'Alessio et al. 1998, 1999; Jang-Condell & Sasselov 2004).

In §2, we summarize the disk model we adopt for this paper and describe the range of parameters we will explore. In §3, we present the results of the parameter study, describe the calculation of truncation radii for the disks, and describe the calculation of the particulate content of the disks. In §4, we discuss our results in the context of both the core accretion

and disk instability models for planet formation, including effects that might enhance the possilibity of planet formation. In §5, we present our conclusions.

2. Model Description

The calculation for the disk models analyzed in this paper is described in detail in Jang-Condell & Sasselov (2003, 2004), and summarized in the appendix. We assume an α-disk model, where the viscosity ν is given by $\nu = \alpha c_s H$ where c_s is the sound speed, H is the thermal scale height of the disk, and α is a dimensionless parameter (Shakura & Sunyaev 1973; Pringle 1981). The temperature of the disk is set by stellar irradiation at the surface and viscous heating at the midplane. The radial and vertical density and temperature structure of the disk is calculated iteratively to achieve self-consistency. We adopt stellar parameters of mass $M_* = 1\ \mathrm{M}_\odot$, temperature $T_* = 4280$ K, and radius $R_* = 2.6\ \mathrm{R}_\odot$, corresponding to a 1 Myr old star with metallicity $Z = 0.02$ (Siess et al. 2000).

The two remaining free parameters for our disk models are the mass accretion rate onto the star, $\dot{M}$, and the viscosity parameter, α. Accretion rates of T Tauri stars are calculated by subtracting template spectra from the observed spectra and assuming that the excess optical and near-ultraviolet continuum flux comes from the accretion shock caused by disk material falling onto the stellar surface (Gullbring et al. 1998). Typical accretion rates are around $\dot{M} \sim 10^{-9}$–$10^{-7} \mathrm{M}_\odot\,\mathrm{yr}^{-1}$. Values for α are calculated by fitting α-disk models to dust emission from disks at millimeter wavelengths, with a typical value of $\alpha \sim 0.01$ (Hartmann et al. 1998). The D/H ratio in the outer solar system suggests that the early solar nebula may have experienced accretion rates as large as $10^{-5}\mathrm{M}_\odot\,\mathrm{yr}^{-1}$ (Hersant et al. 2001). FU Ori objects may accrete as much as $10^{-4}\ \mathrm{M}_\odot\,\mathrm{yr}^{-1}$, but these are transient phenomena, lasting at most 100 years, so these high accretion rates are not expected to be sustainable in the long run (Calvet et al. 2000; Hartmann & Kenyon 1996). For the sake of argument, we will include an accretion rate of $10^{-4}\ \mathrm{M}_\odot\,\mathrm{yr}^{-1}$ in our suite of models, bearing in mind that this would be an extreme system, not representative of planet-forming disks in general. Given these observational constraints, we calculate a grid of disk models, with α set to 0.001, 0.01 or 0.1, and $\dot{M}$ set to 10^{-4}, 10^{-5}, 10^{-6}, 10^{-7}, 10^{-8} or $10^{-9}\ \mathrm{M}_\odot\,\mathrm{yr}^{-1}$. We calculate the models out to 256 AU, but consider only the material interior to the truncation radius to be available for planet formation. We shall refer to a given disk model by the coordinate pair $(\alpha, \dot{M})$, so that Model $(0.01, 10^{-7})$ refers to the run with $\alpha = 0.01$ and $\dot{M} = 10^{-7}\ \mathrm{M}_\odot\,\mathrm{yr}^{-1}$.

3. Results

3.1. Mass Profiles

The mass profiles of our set of models are shown in Figure 1. The total disk mass is defined as the mass interior to the given radius. Solid, dotted, and dashed lines correspond to $\alpha = 0.001$, 0.01, and 0.1, respectively. Accretion rates are indicated by symbol shape and color: orange hexagons for 10^{-4}, red circles for 10^{-5}, green triangles for 10^{-6}, blue squares for 10^{-7}, cyan stars for 10^{-8}, and magenta asterisks for $10^{-9}\,\mathrm{M}_\odot\,\mathrm{yr}^{-1}$. The points mark the truncation radii of each disk model, as will be discussed in §3.2.

The overall mass of the disk increases with increasing accretion rate and decreasing α. Models $(0.1, 10^{-8})$, $(0.1, 10^{-9})$, and $(0.01, 10^{-9})$ contain less than 10 M_J within 100 AU, so we can rule out these disks as having too little mass to form a Jupiter-mass planet and ignore them for the remainder of this study.

3.2. Disk Truncation Radius

The disk around a protostar will be disrupted by the orbit of a close stellar companion. For the purposes of this paper, we will assume that the pair of stars composing HD 188753B act dynamically as a single object. Supposing that planet formation takes place with the stars in their current orbital configuration, how much will a disk around HD 188753A be truncated? One way to approach the problem is to calculate orbits of test particles to look for stable orbits (Pichardo et al. 2005). This method gives a truncation radius of 1.3 AU, regardless of disk model parameters.

Another method is to analyze resonant torques and approximate the size of the disk to be where resonant and viscous torques balance (AL). In this case, the disk size depends on the Reynolds number, $Re \equiv [(H/r)^2\alpha]^{-1}$, where r is the disk radius. We take $H/r = c_s/(r\Omega_p)$, where $\Omega_p = \sqrt{GM_\star/r^3}$ is the orbital angular speed of the planet. Figures 7 and 8 of AL show truncation radii versus eccentricity and Reynolds number for binary mass ratios of $\mu = 0.1$ and 0.3, where μ is the ratio of the stellar mass to the total binary mass. HD 188753A has an eccentricity of $e = 0.5$ and $\mu = 0.4$. Reading off values from Figures 7 and 8 of AL, we can determine the variation of truncation radii with Reynolds number for $e = 0.5$ and $\mu = 0.1$ or 0.3. We can then extrapolate between these two curves to find truncation radii versus Reynolds number for $\mu = 0.4$.

The Reynolds number in each disk model depends on the input parameters, but stays fairly flat with radius, as shown in Figure 2. The lines are labelled in the same way as in

Figure 1. The dependence of truncation radius on Reynolds number as calculated above is also plotted as a long-dashed line. The apparent break in slope is a result of sampling in Re value: AL calculated truncation radii for integral values of log(Re), so intermediate values need to be interpolated. From the intersection of this line with each model profile, we determine a unique truncation radius for each disk model. These radii and the enclosed disk masses ($M_{\rm disk}$) are tabulated in Table 1.

These truncation radii are systematically larger than those of Pichardo et al. (2005), so we adopt the larger values to be conservative. We have marked the truncation radii for each model on Figure 1 so we can read off the mass of disk material within the truncated disk. Only disks with accretion rates of at least $10^{-7}\,{\rm M}_\odot\,{\rm yr}^{-1}$ contain more than 1 M_J within their truncation radii, ruling out at least half the models. Planet formation is not 100% efficient, so we can probably even rule out accretion rates of less than $10^{-6}\,{\rm M}_\odot\,{\rm yr}^{-1}$.

We shall assume that the disks are dynamically truncated and that irradiation from the stellar companion is negligible compared to heating from viscous accretion and the central star. Inclusion of this irradiation would most likely only further decrease the likelihood of planet formation since it would provide an additional heat source at the outer edge of the disk, inhibiting planet formation by either core accretion or disk instability. In the absence of additional accretion of material past the companion's orbit onto the disk, the disk should be viscously spreading both inwards and outwards. The calculated truncated disk masses should be considered upper limits because of these considerations.

3.3. Disk Characteristics

Table 1 summarizes some of the characteristics of out truncated disk models. For each disk model, we list its truncation radius $r_{\rm tr}$, the mass of the truncated disk $M_{\rm disk}$, the disk lifetime $t_{\rm disk} \equiv M_{\rm disk}/\dot{M}$, and the minimum value for the Toomre Q parameter $Q_{\rm min}$.

Disk lifetime decreases with increasing α and increasing accretion rate. However, all the disk lifetimes are less than 2×10^5 years, whereas core accretion takes several millions of years (Pollack et al. 1996; Inaba et al. 2003; Hubickyj et al. 2005). The presence of a circumbinary disk may provide a reservoir that replenishes the circumstellar disk and extends its lifetime (Artymowicz & Lubow 1996; White & Ghez 2001). AL predict that accretion of circumbinary material should proceed faster onto the smaller-mass star, but observations of binary T Tauri stars appear to refute that (White & Ghez 2001).

The Toomre Q parameter is a measure of whether or not a gaseous disk is locally stable

to axisymmetric perturbations. It is defined as

$$Q = \frac{c_s \kappa}{\pi G \Sigma} \tag{1}$$

where κ is the epicyclic frequency, G is the gravitational constant, and Σ is the local gas surface density of disk (Binney & Tremaine 1987). In a disk with approxmate Keplerian rotation, $\kappa \approx \Omega_K$. In our α-disk models, Q decreases with radius, so $Q_{\rm min}$ is evaulated at $r_{\rm tr}$. We also find that $Q_{\rm min}$ is inversely correlated with $M_{\rm disk}$ – the most massive disks have the lowest values of Q. The criterion for stability against fragmentation is $Q \gtrsim 1$, so all our disks are stable.

3.4. Solid Formation

In order to form a planet by core accretion, there must be sufficient mass of solid material to coagulate into a dense core which can then accrete gas. We use the results of Pollack et al. (1994) for sublimation temperatures and mass fractions of olivines, orthopyroxene, iron, water, troilite, refractory organics and volatile organics, which compose the bulk of the dust in the protoplanetary disks. We take into account the variation of sublimation temperatures with gas density and calculate the total amount of solid material available in the disk as a function of disk size. These results are plotted in Figure 3. The line types correspond to the same models as the line types in Figure 1. The disk models were calculated at intervals of $\Delta \log(r) = \log \sqrt{2}$, which is evidenced as apparent breaks in slope in the disk profiles. The steepening of the slopes toward small r is due to the sublimation of solids with increasing temperature. Truncation radii are indicated by points whose size indicate the relative total masses of the disks. Filled symbols mark those disks with more than 1 M_J total mass, open symbols (and asterisks) mark those below 1 M_J in total mass.

In general, disks with higher accretion rates and lower α are hotter. The disks with the highest accretion rates are therefore depleted in solids, even though they are overall more massive. Lower values of α favor both more massive disks as well as more solid condensation. Models $(0.001, 10^{-7})$ and $(0.001, 10^{-6})$ are the most favorable for planet formation under the core accretion scenario, but even they contain just a few $M_\oplus$ of material. Given that at least 10 $M_\oplus$ are required to form a Jupiter-mass planet, this amount of solid material is insufficient for planet formation (Pollack et al. 1996; Inaba et al. 2003; Hubickyj et al. 2005).

4. Discussion

There are two main paradigms of planet formation – core accretion and disk instability. In core accretion, solid particles grow and aggregate until a body with sufficient mass to accrete gas forms. In disk instability, the disk fragments into gas giant planets. In this section, we address the likelihood of either mechanism taking place in the suite of disk models we have calculated.

4.1. Core Accretion

As discussed in the previous section, none of our disk models contain enough solids within $r_{\rm tr}$ to form a sufficiently massive core to accrete gas. In addition, the lifetimes of the disks are too short for core accretion to occur. However, observations of young binary stars indicate that their disks are often replenished by a circumbinary reservoir of material (Monin et al. 2006). Here, we will attempt to salvage core accretion by extending the disk's lifetime via replenishment and allowing additional solid material filter through the disk. Can a 10 $M_\oplus$ planet core still be assembled under these conditions?

Solid particles can cross the gap between a circumbinary disk and a circumstellar disk if they are small and coupled to the gas. Otherwise they do not lose angular momentum efficiently enough to be captured by the star. This rules out the addition of large planetesimals ($\gtrsim 1$ km) to the circumstellar disk that could be precursors to a large planet embryo – planetesimals must be built up from small dust particles.

As particle sizes increase, they experience drag forces that move them through the disk and may allow local enhancements in solid particle densities (e.g. Youdin & Shu 2002; Youdin & Chiang 2004). When the surface density of particles reaches a critical value, Σ_c, the particles may be able to undergo gravitational instability to quickly form planetesimals. This is not be confused with disk instability, which is when the gas in the disk fragments into gravitationally bound clumps. Disk instability will be discussed later in this paper. We will follow the formalism of Youdin & Shu (2002), ignoring turbulent stresses, for simplicity. Weidenschilling (2003) argues that turbulent stresses would inhibit particle accumulations, which would only further strengthen our result. On the other hand, Youdin & Chiang (2004) find that turbulent stresses should hasten accumulations rather than inhibit them, but since we will be calculating steady state particle densities, our results will not be affected qualitatively.

We define Σ_p as the surface density of solids. When Σ_p reaches a certain critical threshold, turbulent mixing can no longer prevent particles from settling out to the midplane. At

this point, the midplane particle density formally goes to infinity and gravitational instability of the particle layer can result in the rapid formation of large bodies (Sekiya 1998; Youdin & Shu 2002). This critical surface density is

$$\Sigma_c = 2\sqrt{\mathrm{Ri}_c}\eta r \rho_g s(\psi) \tag{2}$$

where $\mathrm{Ri}_c \approx 1/4$ is the Richardson number at the onset of Kelvin-Helmholtz instability, ρ_g is the density of the gas at the midplane, η is fractional velocity differential between the gas and Keplerian rotation

$$\eta \equiv -\frac{\partial P/\partial r}{2\rho_g r \Omega_K^2}, \tag{3}$$

where P is the gas pressure and

$$s(\psi) = (1+\psi)\ln[(1+\psi+\sqrt{1+2\psi})/\psi] - \sqrt{1+2\psi}, \tag{4}$$

where $\psi = 4\pi G\rho_g/\Omega_K^2$.

In Figure 4, we plot Σ_c versus radius for our models as dotted lines. For comparison, we also plot the unperturbed surface density of solids ($\Sigma_{p,0}$) as solid lines. The models are sorted column-wise by α as labelled at the top, and row-wise by accretion rate as labelled on the right. We have omitted $(0.001, 10^{-5})$ and $(0.01, 10^{-5})$ because the temperatures in those disks are everywhere too hot inside of 2.5 AU for any solids to remain. In all our models, $\Sigma_{p,0}$ is at least an order of magnitude below the threshold for gravitational instability to operate.

A particle of radius a is subject to a headwind as it decouples from the gas and tries to orbit at the Keplerian velocity rather than the gas velocity, which is slower due to pressure support (Weidenschilling 1977; Youdin & Shu 2002). The radial drift of the particle can be described by the Epstein drag law:

$$v_{\mathrm{Ep}} = -\frac{t_{\mathrm{st}}}{\rho_g}\frac{\partial P}{\partial r} = 2\eta t_{\mathrm{st}}\Omega_K^2 r \tag{5}$$

where the stopping time is defined as

$$t_{\mathrm{st}} = \frac{\rho_s a}{\rho_g c_s} \tag{6}$$

where ρ_s is the bulk density of the particle.

Does Σ_p ever exceed the critical density for gravitational instability to operate? To answer this question, we need to calculate how Σ_p evolves according to the drift rates calculated above. We will assume that the gas, which composes the bulk of the mass in the disk,

is unperturbed by the movement of the solid particles. Our assumptions will be as generous as possible toward the onset of gravitational instability in order to put firm constraints on core formation. We calculate the evolution of Σ_p in each of our disk models interior to 2.5 AU, and assume that the amount of solids at the outer boundary is held constant by replenishment from some external reservoir, such as a circumbinary disk.

The continuity equation for Σ_p can be written as

$$r\frac{\partial \Sigma_p}{\partial t} = \frac{\partial}{\partial r}(r\Sigma_p v_{\rm r}). \tag{7}$$

where v_r is the inward radial velocity of the particle. In steady state, the left side of equation (7) vanishes. In principle, the time evolution of Σ_p may result in significant transient increases locally in the disk. However, for the following analysis, we have calculated both the time-dependent and steady-state Σ_p and find that the time for relaxation to steady state is shorter than the calculated disk lifetimes, and there are no significant transient spikes in the density profile.

The constant of integration for the right side of equation (7) is essentially the mass flow rate of solids through the disk, which is set by the boundary condition of the rate of replenishment of solids at the outer edge of the disk, $dM_p/dt \equiv 2\pi r v_r \Sigma_p$. However, we also need to take into account the sublimation of solids as they fall inwards into regions of higher temperatures and pressures. If we define $f(r)$ to be the equilibrium mass fraction of solids to total disk material at the midplane temperature and density, then

$$\Sigma_p = \frac{f(r)}{2\pi r v_r f(r_{\rm o})}\frac{dM_p}{dt}. \tag{8}$$

where $r_{\rm o} = 2.5$ AU is the outer radius of the disk.

If we assume that the steady state particle inflow rate is given by holding $\Sigma_p(r_{\rm o})$ constant and setting $v_r = v_{\rm Ep}$, then

$$\Sigma_{p,d} = \frac{r_{\rm o} v_{\rm Ep}(r_{\rm o})}{r v_{\rm Ep}} f(r)\Sigma(r_{\rm o}). \tag{9}$$

where the subscript d indicates that we have assumed that $v_r = v_{\rm Ep}$. The quantity $v_{\rm Ep}(r_{\rm o})/v_{\rm Ep}$ is independent of a, so the total pileup particle density integrated over a depends only on the characteristics of the unperturbed disk, not on the size distribution of particles. In Figure 4, we plot $\Sigma_{p,d}$ for each of our models as a dot-dashed line. Although there is some steepening of the density profile toward smaller radii, it is not enough to raise the surface density of solids above the critical threshold for any disk model at any radius.

A different way to treat the boundary condition is that the disk is being replenished at a rate equal to that accretion rate, so $dM_p/dt = f(r_{\rm o})dM/dt$. In this case, we need to take

into account the radial velocity of the gas itself, which is being accreted onto the star. The smaller particles remain coupled to the gas, and leaving out the gas velocity would result in an unphysical accumulation of the smallest particles at the disk's outer edge. For a constant accretion rate, the radial velocity of the gas is

$$v_{\rm gas} = \frac{dM/dt}{2\pi r\Sigma} \tag{10}$$

and the total radial velocity of the particles is $v_r = v_{\rm gas} + v_{\rm Ep}$. The equation for the steady-state surface density of particles of size a is

$$\Sigma_{p,g}(a) = \frac{f(r)}{2\pi r(v_{\rm gas} + v_{\rm Ep})}\frac{dM}{dt}m(a) \tag{11}$$

where $m(a)$ is the normalized mass distribution of particles of size a and the subscript g refers to the gas velocity being accounted for. If we assume the bulk density of the particles is constant and the number density of particles with radii between a and $a + da$ is $n(a)da \propto a^{-p}da$, then

$$m(a) = \frac{(4-p)a^{3-p}}{a_{\rm max}^{(4-p)} - a_{\rm min}^{(4-p)}} \approx \frac{(4-p)a^{3-p}}{a_{\rm max}^{(4-p)}} \tag{12}$$

for $p < 4$ and $a_{\rm max} \gg a_{\rm min}$. The parameters for our dust model are $p = 3.5$ with $a_{\rm max} = 1$mm and $a_{\rm min} = 5 \times 10^{-3}\,\mu$m. Then,

$$\Sigma_{p,g}(r) = \frac{f(r)\dot{M}}{2\pi r}[v_{\rm gas}v_{\rm Ep}(a_{\rm max})]^{-0.5}\left[\arctan\sqrt{\frac{v_{\rm Ep}(a_{\rm max})}{v_{\rm gas}}} - \arctan\sqrt{\frac{v_{\rm Ep}(a_{\rm min})}{v_{\rm gas}}}\right]. \tag{13}$$

In Figure 4, we plot $\Sigma_{p,g}$ for each of our models as a dashed line. For the higher accretion rates, $\Sigma_{p,g}$ differs little from $\Sigma_{p,0}$. This is because the radial velocity of the gas is higher than the radial velocity of the dust, so the movement of the gas dominates the flow. At lower accretion rates, $\Sigma_{p,g}$ actually falls below $\Sigma_{p,0}$ because the dust is being swept in ahead of the gas. This is accompanied by a slight steepening of the profile. Although there is some transient accumulation of solids as the density profile evolves to steady state, it is small and never approaches Σ_c. This analysis omits many important physical processes such as magnetic fields, grain growth beyond 1 mm, and radiation pressure, but any process that would allow for gravitional instability to occur would have to increase the surface density by more than an order of magnitude.

Alternatively, kilometer-sized planetesimals can form via grain-grain collisions in about 10^4 years at 1 AU in the early solar nebula, assuming perfect sticking in collisions (Weidenschilling & Cuzzi 1993). This also assumes that they grow quickly past 1-100 cm in size, because particles of that size spiral into the star on the order of 100 years (Weidenschilling

1977). In this scenario, planetesimals form out of the dust that is carried in with the gas from the outer reservoir. Once they reach about a kilometer in size, they decouple from the gas. As more material comes in from the the circumbinary reservoir, the population of kilometer-sized bodies grows. They collide with each other and coaslesce until a planet core is built up. However, growth of this planet core is limited by the size of the feeding zone and by the amount of solids available. Most simulations of giant planet core formation in the early solar nebula are set at 4-5 AU because the feeding zone is sufficiently large and the solid abundance is enhanced by ice formation at those distances (e.g. Pollack et al. 1996). This is well outside the disk truncation radius for HD 188753A. Moreover, stirring by the eccentric binary companion will raise relative velocities between planetesimals, increasing the likelihood that collisions will result in disruption of bodies rather than coalescence (Thébault et al. 2006). A detailed simulation of this process is outside the scope of this paper, so we will rule planet formation in HD 188753 via core accretion unlikely, but not impossible.

4.2. Disk Instability

Since disk instability can occur within a thousand years, perhaps this is a more plausible mechanism for planet formation (e.g. Boss 2001). If $Q \lesssim 1$, disk instability can operate – that is, the disk needs to be sufficiently cold and/or massive in order for gravitationally bound clumps to form. The minimum Q is shown for our various disk models in Table 1. For all the disk models, Q is above the stability threshold of $Q \gtrsim 1$.

Boss (2001) shows that disk instability can act in disks that are only marginally stable, with $Q \approx 1.5$, which the disk model $(0.001, 10^{-4})$ achieves at its outer edge. In Figure 5, we plot the variation of Q with distance from the star for the disk models with the lowest values of Q. Note that Q increases rapidly as the gas moves inward as the disk gets accreted by the star. As discussed before, accretion rates of $10^{-4}\,\mathrm{M}_{\odot}\,\mathrm{yr}^{-1}$ are observed only as transient phenomena in young stars, lasting less than 100 years. Simulations show disk instability acting in several hundreds of years, so even disk instability may not proceed fast enough to create a giant planet (Boss 2001). This disk model has a lifetime of only 3000 years, which also limits the timescale for planet formation. The parts of the disk that are marginally unstable at the outer edge accrete inward rapidly to where Q is well above the stability threshold.

The eccentric stellar companion to HD 188753 could excite spiral density waves in the disk, increasing the surface density in parts of the disk. Since Q varies inversely with Σ, local enhancements of the surface density may make parts of the disk unstable to gravitational collapse. The most massive disk models also have the smallest values of Q, so planets may

be able to form if density waves can create sufficient density enhancements. On the other hand, shock heating raises the temperature of the disks, which in turn raises Q.

A number of simulations of triggered planet formation in binary disks have been carried out. Boss (2006) shows that a binary companion can trigger disk fragmentation, whereas Nelson (2000) finds that shock heating inhibits disk fragmentation. The difference between these results is in cooling times – short cooling times lead to clump formation while long cooling times inhibit it. Mayer et al. (2005) examine a range of cooling times for their simulations and conclude that shock-heating inhibits fragmentation in general, except for the shortest cooling times. All these simulations were carried out in disks that were already only marginally stable, with $Q \sim 1.4$, and were subject to fragmentation even in isolation, being cooler and larger than the ones we have modelled here. Moreover, Mayer et al. (2005) find that fragmentation is inhibited by the presence of a binary companion in more massive disks, even if they form clumps in isolation. All the disks considered in this study are above the stability threshold of $Q \sim 1.4$. The disks with the lowest values of Q are also the most massive, so we conclude that the presence of the binary companion does not enhance disk fragmentation, but may even do the opposite. Thus, we can rule out planet formation by disk instability.

5. Conclusions

The in situ formation of HD 188753's planet appears to be unlikely according to current models of planet formation. Assuming a simple truncated α-disk model for the protoplanetary disk around HD 188753A, we have studied a range of disk parameters that are representative of observed protoplanetary disks and found that even if we can model a disk with sufficient total mass within the disk truncation radius, its timescales are too short, it contains insufficient solids, and it is too hot for planets to form by generally accepted mechanisms.

A steady-state disk around HD 188753 does not contain enough solids to form a massive enough core to accrete a gaseous envelope. If the disk is replenished by a circumbinary reservoir, enough solids could be delivered to the circumstellar disk to assemble a protoplanetary core, in principle. However, the temperature of the disk and the sitrring by the eccentric binary make it a hostile environment in which to assemble this core.

Disk instability not well-favored either. The only disk model that is even marginally unstable to fragmentation has an accretion rate of 10^{-4} $M_\odot\,yr^{-1}$, which is only seen in extreme, transient systems, namely FU Ori outbursts. The instability is favored only in the outer reaches of the disk, which are most subject to perturbation and disruption by the

eccentric companion.

Admittedly, an α-disk model is a very simple system and real disks are likely to be much more complex than the model predicts. However, it is still a useful tool for analyzing some of the properties of protoplanetary disks. A close stellar companion will create additional complexity to the disk model, introducing highly non-axisymmetric structures such as spiral waves which cannot be adequately modelled by a simple α-disk. Excitation of spiral density waves is more likely to disrupt planet formation than enhance it through shock heating, which will sublimate dust particles and elevate Q. The eccentric stellar companion is also likely to stir up any forming planetesimals and destroy them by smashing them into each other. To adequately model these effects, however, requires a high-resolution hydrodynamic simulation, which is beyond the scope of this paper.

Many thanks go to John Chambers, Dimitar Sasselov, Alan Boss, and Alycia Weinberger for helpful discussions and comments in the preparation of this paper. This research was supported by the NASA Astrobiology Institute under Cooperative Agreement NNA04CC09A.

A. Detailed Disk Structure

The disk model has been described in detail in Jang-Condell & Sasselov (2003, 2004), but a summary is provided in this section. We adopt the formalism developed by Calvet et al. (1991) and D'Alessio et al. (1998, 1999), with some simplifying assumptions. We use the opacities from D'Alessio et al. (2001) using a dust model with parameters $a_{\max} = 1\,\mathrm{mm}$, $T = 300$ K, and $p = 3.5$, assuming that the dust opacities are constant throughout the disk. The values for the opacities (in $\mathrm{cm^2 g^{-1}}$) are as follows: the Rosseland mean opacity is $\chi_R = 1.91$, the Planck mean opacity at disk-temperature (300 K) wavelengths is $\kappa_P = 0.992$, and the Planck mean opacities at stellar-temperature (4000 K) wavelengths are $\chi_P^* = 5.86$ and $\kappa_P^* = 1.31$. The fraction of stellar radiation that is absorbed is represented by the absorption coefficient, $\alpha_{abs} = \kappa_P^*/\chi_P^*$, while the scattered fraction is $\sigma = 1 - \alpha_{abs}$.

We assume that the disk is locally plane parallel to decouple the radial and vertical dependencies of the disk properties. For a given radius r, the vertical structure is calculated as follows. The optical depth is given by

$$\tau_d(z) = \int_z^{z_\infty} \chi_R \rho(z') dz'. \tag{A1}$$

The density and temperature are calculated assuming hydrostatic equilibrium,

$$\frac{dP}{dz} = -\rho \frac{GM_* z}{r^3}. \tag{A2}$$

We assume the ideal gas law, $P = \rho kT/\bar{m}$, where k is the Boltzmann constant and $\bar{m}$ is the mean molecular weight of the gas, which we assume to be primarily molecular hydrogen.

The temperature in the disk as a function of optical depth and angle of incidence of stellar radiation μ_s can be expressed as

$$T(\tau_d, \mu_s) = [T_v^4(\tau_d) + T_r^4(\tau_d, \mu_s)]^{1/4} \tag{A3}$$

where T_v and T_r are temperatures due solely to viscous heating and stellar irradiation, respectively.

We assume that viscous flux is generated at the midplane and transported radiatively in a grey atmosphere so that

$$T_v = \left[\frac{3F_v}{8\sigma_B}(\tau_d + 2/3)\right]^{1/4} \tag{A4}$$

where σ_B is the Stefan-Boltzmann constant. The viscous flux F_v at a distance r for a star of mass $M_\star$ and radius $R_\star$ accreting at a rate $\dot{M}_a$ is

$$F_v = \frac{3GM_\star\dot{M}_a}{4\pi r^3}\left[1 - \left(\frac{R_\star}{r}\right)^{1/2}\right] \tag{A5}$$

(Pringle 1981).

Since we have assumed that the opacities are constant throughout, the optical depth to stellar frequencies is related to the optical depth to disk frequencies as $\tau_s = (\chi_P^*/\chi_R)\tau_d$. The equation for T_r is

$$\frac{\sigma_B T_r^4}{\pi} = \frac{\alpha_{abs}F_{irr}\mu_s}{4\pi}\left[c_1 + c_2 e^{-\tau_s/\mu_s} + c_3 e^{-\beta\tau_s}\right], \tag{A6}$$

where we define $\beta = \sqrt{3\alpha_{abs}}$ to get

$$c_1 = \frac{6 + 9\mu_s\chi_R/\chi_P^*}{\beta^2} - \frac{6(1 - \chi_R/\chi_P^*)\,(3 - \beta^2)}{\beta^2(3 + 2\beta)(1 + \beta\mu_s)} \tag{A7}$$

$$c_2 = \left(\frac{\chi_P^*}{\mu_s\kappa_P} - \frac{3\mu_s\chi_R}{\chi_P^*}\right)\frac{(1 - 3\mu_s^2)}{(1 - \beta^2\mu_s^2)} \tag{A8}$$

$$c_3 = \left(\frac{\beta\chi_P^*}{\kappa_P} - \frac{3\chi_R}{\chi_P^*\beta}\right)\frac{(2 + 3\mu_s)(3 - \beta^2)}{\beta(3 + 2\beta)(1 - \beta^2\mu_s^2)}. \tag{A9}$$

The upper boundary condition is set so that $P(z_\infty) = 10^{-10}$ dyne, and we integrate the equations for τ_d, ρ, and T down to the midplane using some initial guess for z_∞. The other boundary condition is that we match the total integrated surface density

$$\Sigma = \int_{-z_\infty}^{z_\infty} \rho\, dz' \tag{A10}$$

with the surface density given by a steadily accreting viscous disk

$$\Sigma = \frac{\dot{M}}{3\pi\nu}\left[1 - \left(\frac{R_\star}{r}\right)^{1/2}\right] \tag{A11}$$

(Pringle 1981). We adopt a standard Shakura-Sunyaev viscosity with $\nu = \alpha c_s H$ (Shakura & Sunyaev 1973). Depending on the difference between equation (A10) and equation (A11), we adjust our guess for z_∞ until the values for Σ converge.

The angle of incidence, μ_s, depends on slope of surface dz_s/dr, where z_s is the "surface" of the disk, where $\tau_s/\mu_s = 2/3$. To get a self-consistent answer for μ_s we iteratively calculate the vertical structure of the disk at intervals of $\Delta \log r = \frac{1}{2}\log 2$, calculating the slope of the surface between intervals of r. For completeness, the disk models are calculated out to 256 AU, even though only the inner few AU are relevant for this study.

REFERENCES

Artymowicz, P. & Lubow, S. H. 1994, ApJ, 421, 651

—. 1996, ApJ, 467, L77

Binney, J. & Tremaine, S. 1987, Galactic dynamics (Princeton, NJ, Princeton University Press, 1987, 747 p.)

Boss, A. P. 1997, Science, 276, 1836

—. 2000, ApJ, 536, L101

—. 2001, ApJ, 563, 367

—. 2006, ApJ, 641, 1148

Calvet, N., Hartmann, L., & Strom, S. E. 2000, Protostars and Planets IV, 377

Calvet, N., Patino, A., Magris, G. C., & D'Alessio, P. 1991, ApJ, 380, 617

Chambers, J. E. 2004, Earth and Planetary Science Letters, 223, 241

D'Alessio, P., Calvet, N., & Hartmann, L. 2001, ApJ, 553, 321

D'Alessio, P., Calvet, N., Hartmann, L., Lizano, S., & Cantó, J. 1999, ApJ, 527, 893

D'Alessio, P., Canto, J., Calvet, N., & Lizano, S. 1998, ApJ, 500, 411

Gullbring, E., Hartmann, L., Briceno, C., & Calvet, N. 1998, ApJ, 492, 323

Hartmann, L., Calvet, N., Gullbring, E., & D'Alessio, P. 1998, ApJ, 495, 385

Hartmann, L. & Kenyon, S. J. 1996, ARA&A, 34, 207

Hersant, F., Gautier, D., & Huré, J. 2001, ApJ, 554, 391

Hubickyj, O., Bodenheimer, P., & Lissauer, J. J. 2005, Icarus, 179, 415

Inaba, S., Wetherill, G. W., & Ikoma, M. 2003, Icarus, 166, 46

Jang-Condell, H. & Sasselov, D. D. 2003, ApJ, 593, 1116

—. 2004, ApJ, 608, 497

Konacki, M. 2005, Nature, 436, 230

Mayer, L., Wadsley, J., Quinn, T., & Stadel, J. 2005, MNRAS, 363, 641

Monin, J.-L., Clarke, C. J., Prato, L., & McCabe, C. 2006, in Protostars and Planets V, ed. B. Reipurth, D. Jewitt, & K. Keil

Nelson, A. F. 2000, ApJ, 537, L65

Pfahl, E. 2005, ApJ, 635, L89

Pichardo, B., Sparke, L. S., & Aguilar, L. A. 2005, MNRAS, 359, 521

Pollack, J. B., Hollenbach, D., Beckwith, S., Simonelli, D. P., Roush, T., & Fong, W. 1994, ApJ, 421, 615

Pollack, J. B., Hubickyj, O., Bodenheimer, P., Lissauer, J. J., Podolak, M., & Greenzweig, Y. 1996, Icarus, 124, 62

Portegies Zwart, S. F. & McMillan, S. L. W. 2005, ApJ, 633, L141

Pringle, J. E. 1981, ARA&A, 19, 137

Sekiya, M. 1998, Icarus, 133, 298

Shakura, N. I. & Sunyaev, R. A. 1973, A&A, 24, 337

Siess, L., Dufour, E., & Forestini, M. 2000, A&A, 358, 593

Thébault, P., Marzari, F., & Scholl, H. 2006, Icarus, 183, 193

Weidenschilling, S. J. 1977, MNRAS, 180, 57

—. 2003, Icarus, 165, 438

Weidenschilling, S. J. & Cuzzi, J. N. 1993, in Protostars and Planets III, ed. E. H. Levy & J. I. Lunine, 1031–1060

White, R. J. & Ghez, A. M. 2001, ApJ, 556, 265

Youdin, A. N. & Chiang, E. I. 2004, ApJ, 601, 1109

Youdin, A. N. & Shu, F. H. 2002, ApJ, 580, 494

Table 1. Calculated values for the disk models

α	$\dot{M}$ ($M_\odot\,yr^{-1}$)	r_{tr} (AU)	M_{disk} ($M_\odot$)	t_{disk} (yr)	Q_{min}
0.001	10^{-4}	2.0	3.0×10^{-1}	3.0×10^{3}	1.5
0.001	10^{-5}	1.9	7.0×10^{-2}	7.0×10^{3}	4.1
0.001	10^{-6}	1.8	1.6×10^{-2}	1.6×10^{4}	11
0.001	10^{-7}	1.7	3.8×10^{-3}	3.8×10^{4}	30
0.001	10^{-8}	1.6	8.7×10^{-4}	8.7×10^{4}	83
0.001	10^{-9}	1.5	1.9×10^{-4}	1.9×10^{5}	300
0.01	10^{-4}	2.3	5.8×10^{-2}	5.8×10^{2}	6.3
0.01	10^{-5}	2.2	1.3×10^{-2}	1.3×10^{3}	17
0.01	10^{-6}	2.0	3.0×10^{-3}	3.0×10^{3}	48
0.01	10^{-7}	1.9	7.0×10^{-4}	7.0×10^{3}	130
0.01	10^{-8}	1.8	1.6×10^{-4}	1.6×10^{4}	380
0.1	10^{-4}	2.7	1.1×10^{-2}	1.1×10^{2}	26
0.1	10^{-5}	2.5	2.6×10^{-3}	2.6×10^{2}	72
0.1	10^{-6}	2.3	5.9×10^{-4}	5.9×10^{2}	200
0.1	10^{-7}	2.2	1.3×10^{-4}	1.3×10^{3}	560

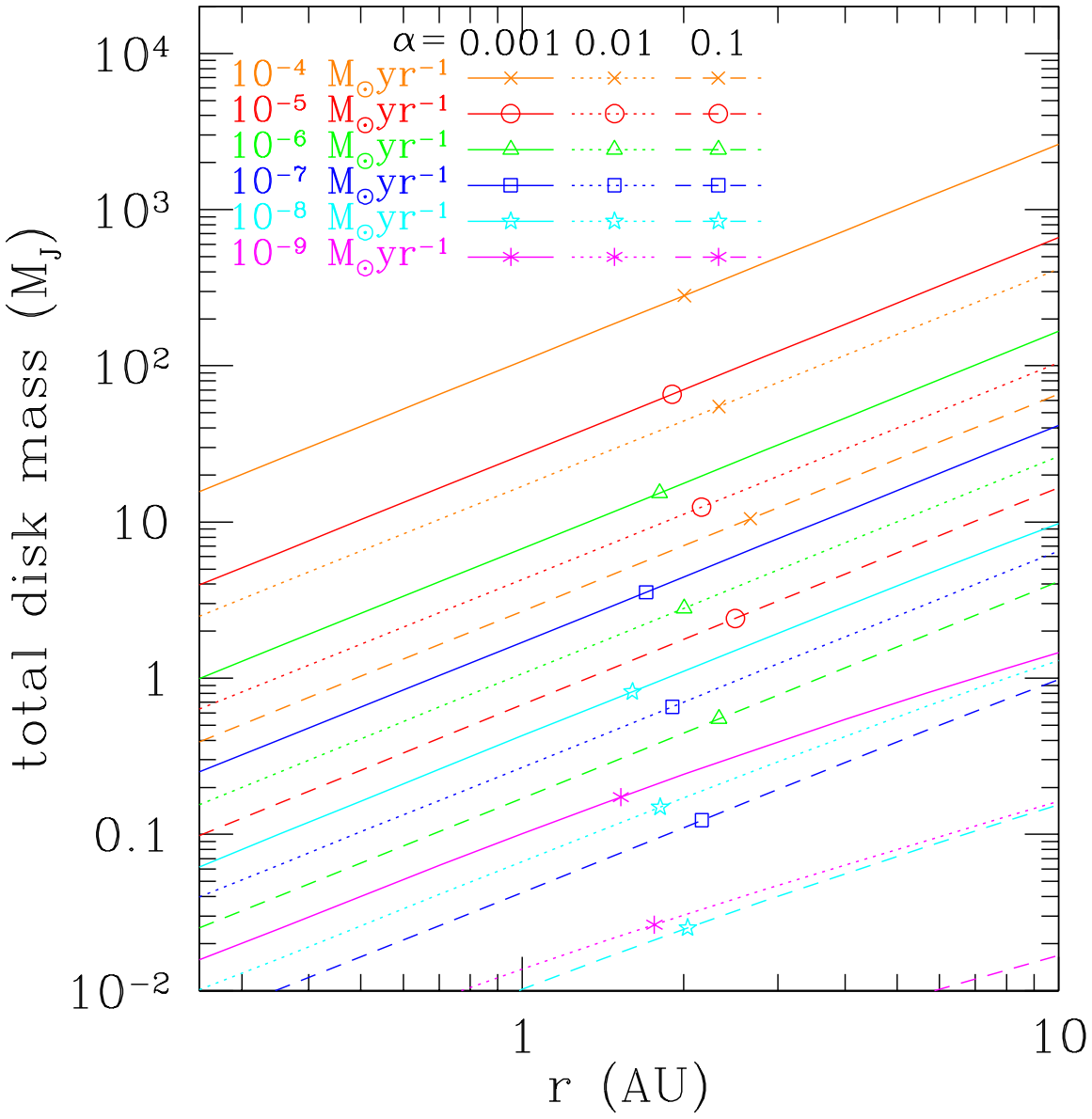

Fig. 1.— Enclosed disk mass versus radius for the suite of calculated disk models, in units of Jupiter masses. The accretion rate is indicated by color and symbol type: orange hexagons for 10^{-4}, red circles for 10^{-5}, green triangles for 10^{-6}, blue squares for 10^{-7}, cyan stars for 10^{-8}, and magenta asterisks for 10^{-9} $M_\odot\,yr^{-1}$. Models with α of 0.001, 0.01 and 0.01 are indicated by solid, dotted and dashed lines, respectively. The locations of the points mark the truncation radius for each disk model.

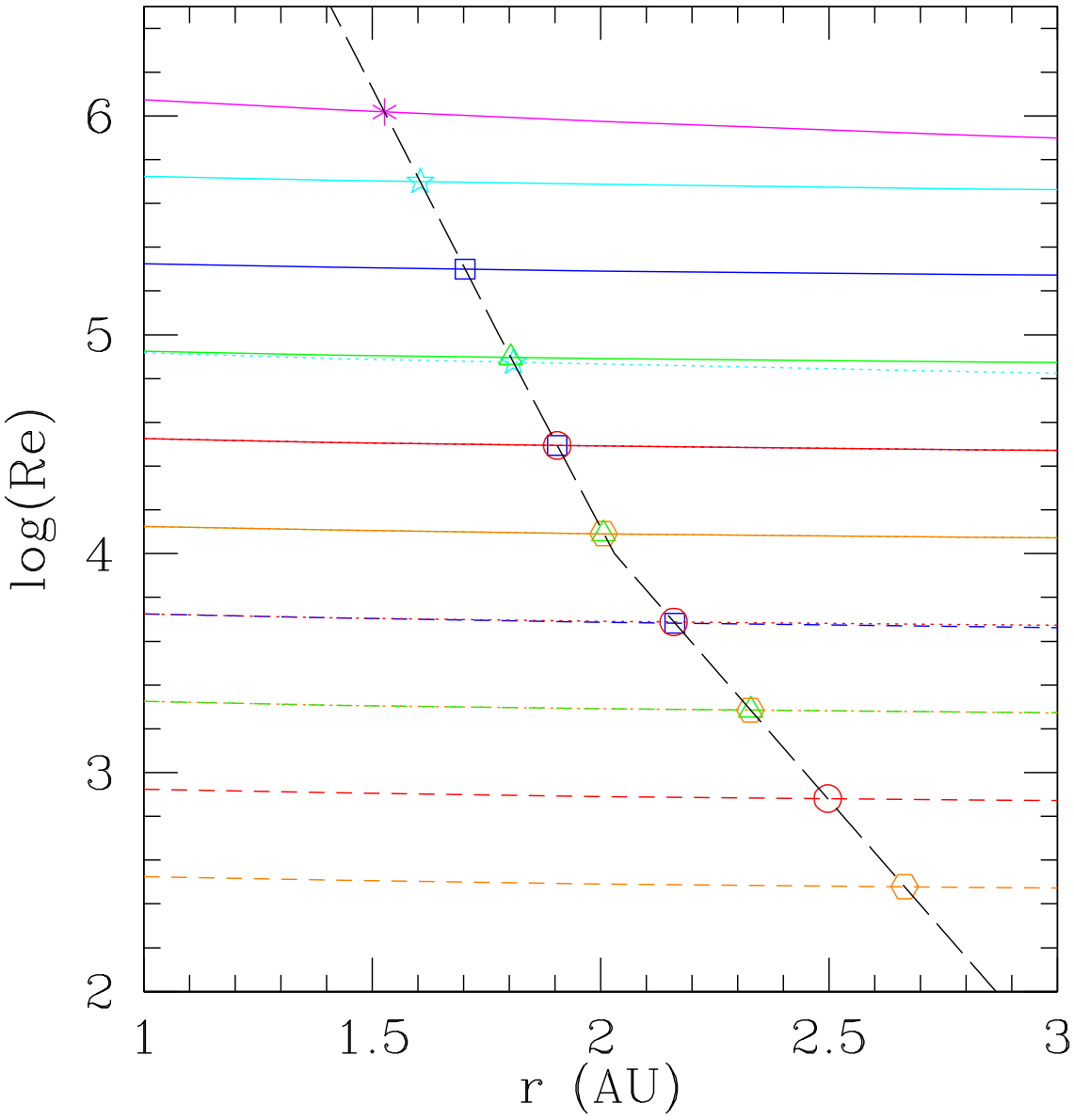

Fig. 2.— Reynolds number versus disk radius for our calculated disk models. The lines are labelled in the same way as Figure 1. The black long-dashed line illustrates the dependence of the truncation radius (horizontal axis) varies with Reynolds number (vertical axis) as calculated following AL for the parameters relevant to the HD 188753 system. The intersection of this line with the line corresponding to each of the disk models is the truncation radius for that model.

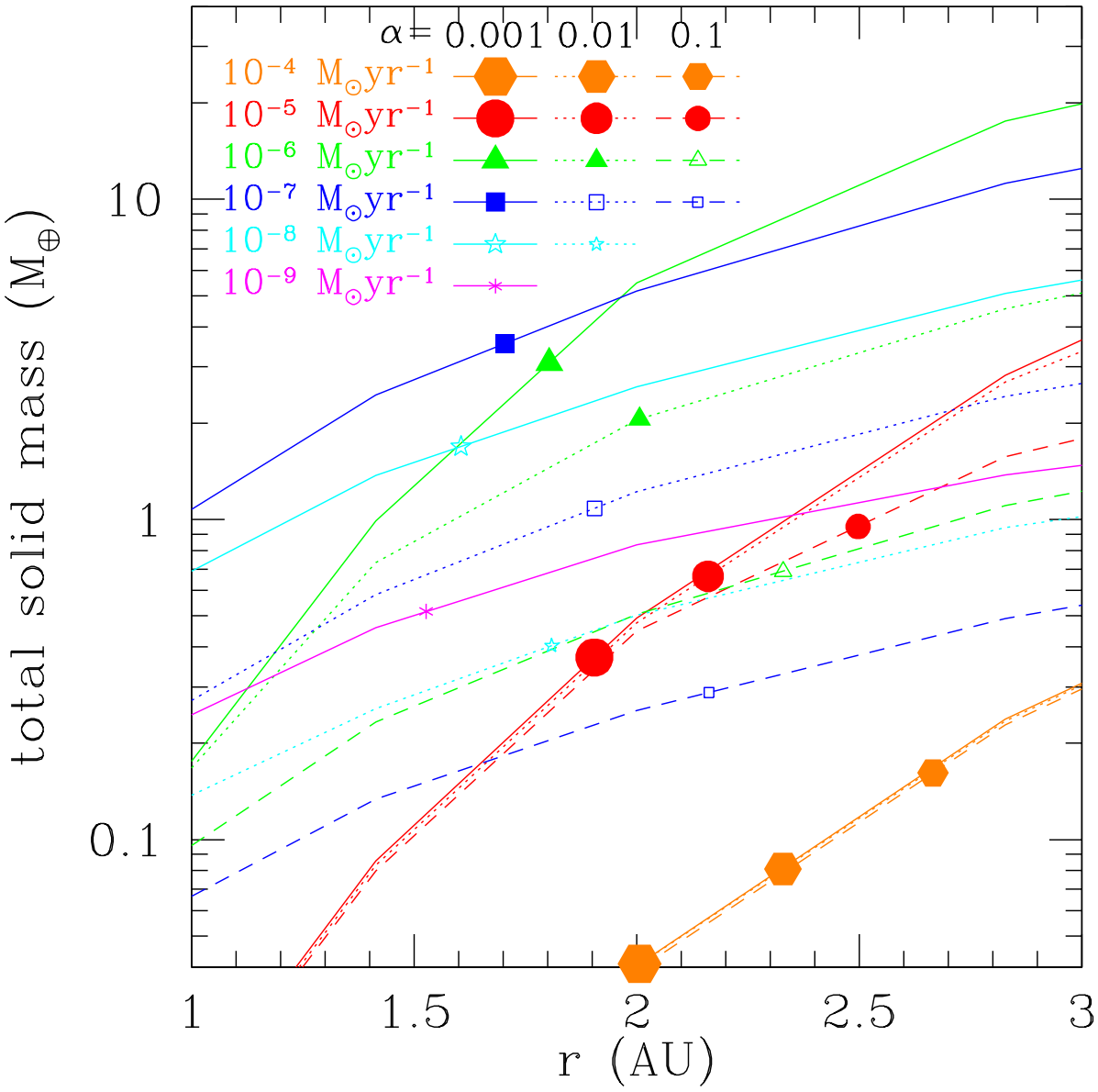

Fig. 3.— Total amount of solid material, in earth masses, available for core formation versus enclosing radius. The lines are labelled in the same way as Figure 1. The points mark the truncation radius for each disk model, with the size of the triangle indicating the relative overall disk mass. Filled (open) triangles mark disks containing more than (less than) 1 M_J.

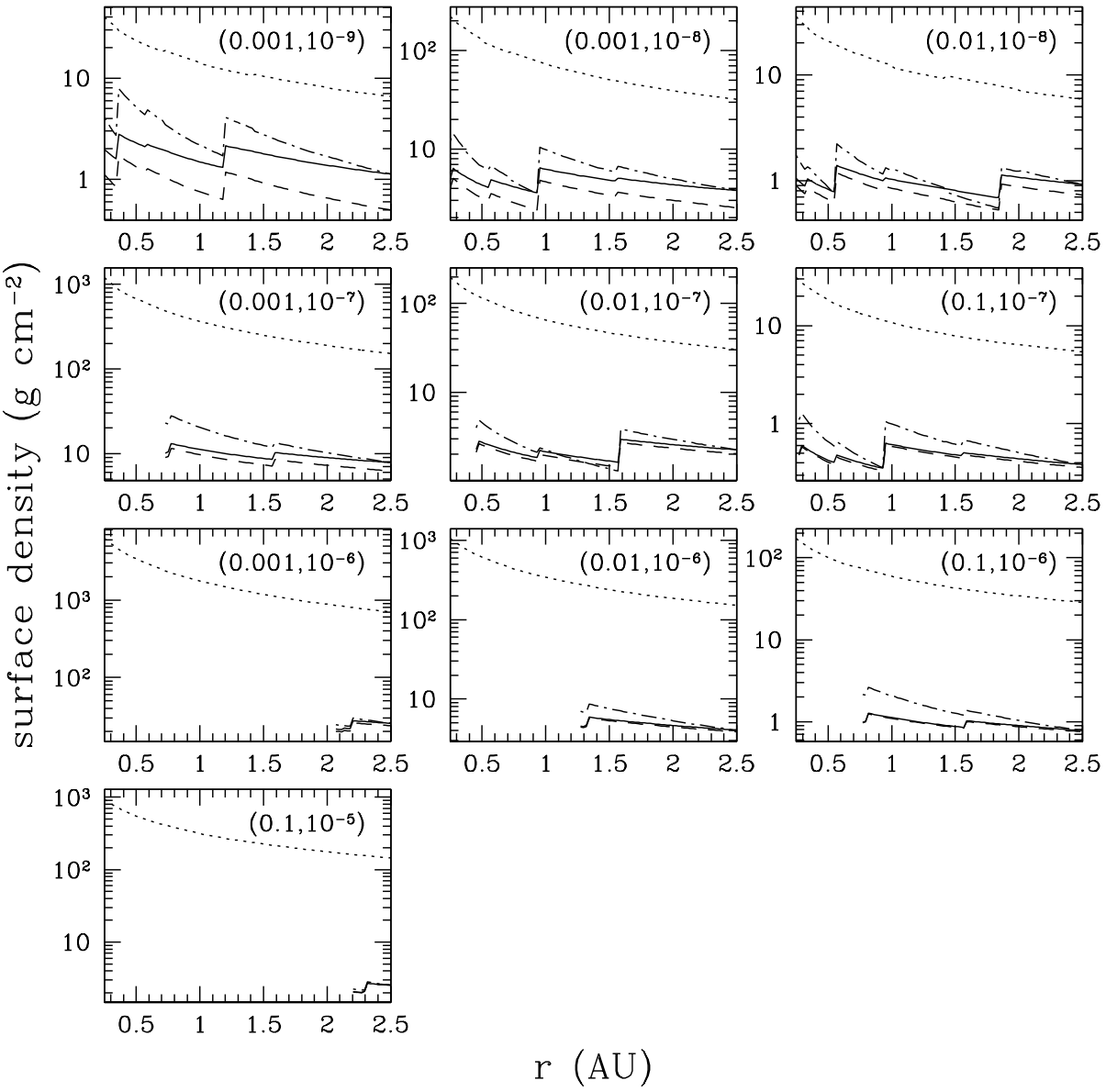

Fig. 4.— Surface densities of solids as a function of distance from the star for planetesimal formation via disk instability, for each model disk as labelled. In each plot, the solid line shows the initial surface density of solids, $\Sigma_{p,0}$. The dotted line shows Σ_c, the critical surface density required for disk instability to occur. The dot-dashed line shows $\Sigma_{p,d}$, the steady-state surface density of solids assuming that all the particles spiral in with a drift rate of $dr/dt = v_{\rm Ep}$. The dashed line shows $\Sigma_{p,g}$, the steady-state surface density of solids assuming that particles drift inward as $dr/dt = v_{\rm gas} + v_{\rm Ep}$. The models $(0.001, 10^{-5})$, $(0.01, 10^{-5})$, and all those accreting at $10^{-4}\,{\rm M}_\odot\,{\rm yr}^{-1}$ are too hot for any solids to form inside of 2.5 AU.

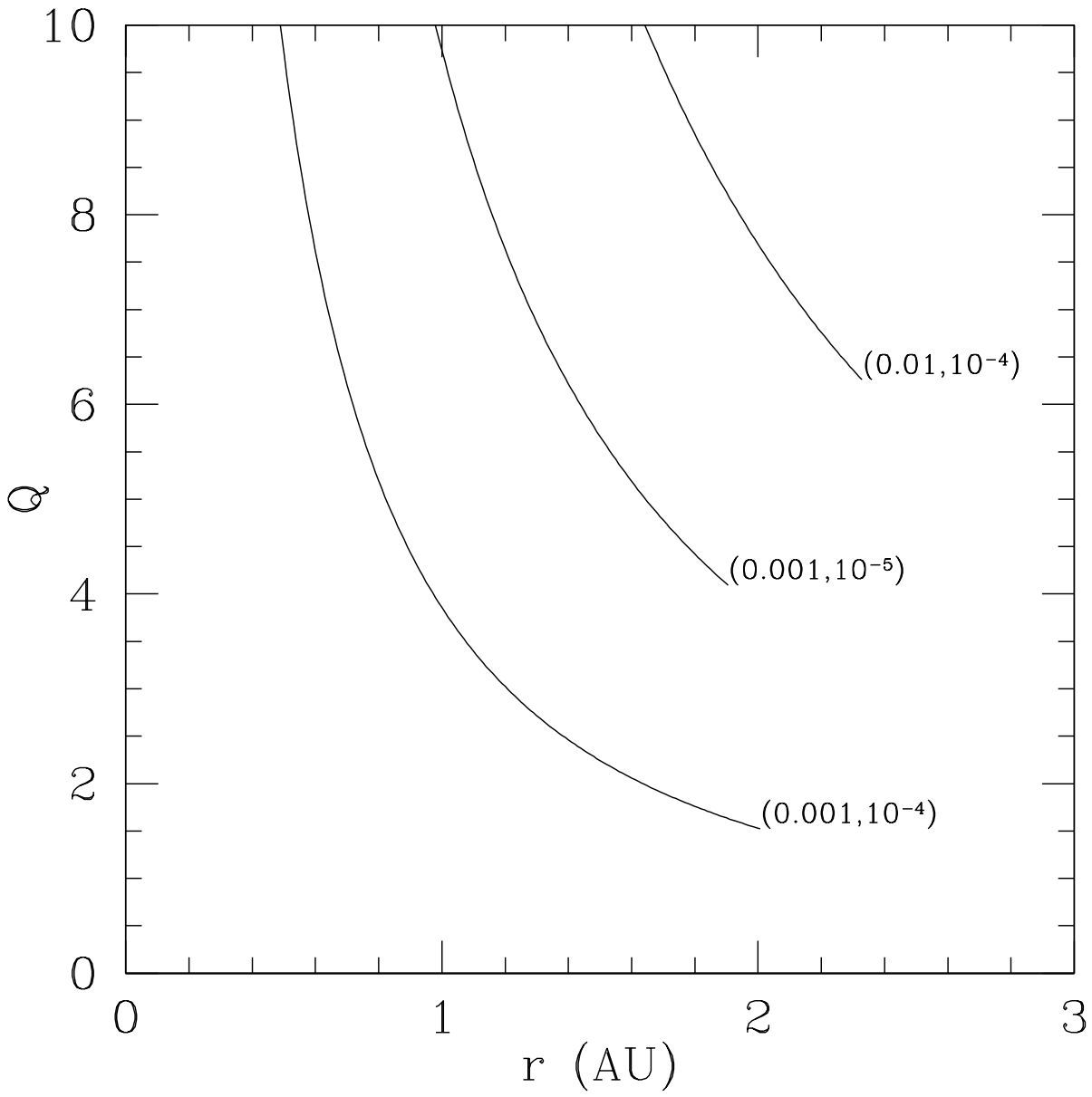

Fig. 5.— Toomre Q parameters versus radius for those disk models with the lowest values of Q.